Progress In Electromagnetics Research, Vol. 113, 161–177, 2011

CALCULATION AND OPTIMIZATION OF ELECTROMAGNETIC RESONANCES AND LOCAL INTENSITY ENHANCEMENTS FOR PLASMON METAMATERIALS WITH SUB-WAVELENGTH DOUBLE-SLOTS

L. Han †

College of Optical Sciences
The University of Arizona, Tucson, Arizona 85721, USA

S. Chen ‡

The Key Laboratory of Weak Light Nonlinear Photonics
Ministry of Education, TEDA Applied Physics School
and School of Physics, Nankai University, Tianjin 300457, China

A. Schülzgen §

College of Optical Sciences
The University of Arizona, Tucson, Arizona 85721, USA

Y. Zeng

Department of Electrical Engineering
Pennsylvania State University, State College
Pennsylvania 16802, USA

F. Song and J. Tian

The Key Laboratory of Weak Light Nonlinear Photonics
Ministry of Education, TEDA Applied Physics School
and School of Physics, Nankai University, Tianjin 300457, China

N. Peyghambarian

College of Optical Sciences
The University of Arizona, Tucson, Arizona 85721, USA

Received 6 December 2010, Accepted 12 January 2011, Scheduled 1 February 2011
Corresponding author: Lin Han (hanlin2003@mail.nankai.edu.cn).

† Also with The Key Laboratory of Weak Light Nonlinear Photonics, Ministry of Education, TEDA Applied Physics School & School of Physics, Nankai University, Tianjin 300457, China.

‡ Also with College of Optical Sciences, University of Arizona, Tucson, Arizona 85721, USA.

§ Also with CREOL, College of Optics and Photonics, University of Central Florida, Orlando, Florida 32816, USA.

Abstract—We propose two metamaterials with sub-wavelength double-slots — single-side double-slot metamaterial and double-side double-slot metamaterial. The dependence of the electromagnetic resonances and local intensity enhancements on the structural parameters is studied by the finite-difference time-domain technique and the finite element method. Results show that the central-arm of a double-slot structure strongly influences frequency and local intensities at both high- and low-frequency resonances. Very strong field localization can be achieved at the high-frequency resonance and its particular distribution can be well controlled by the width of the central-arm. A double-side double-slot structure can be utilized to separately enhance the high-frequency resonance, while suppressing the low-frequency resonance. The simulation results are discussed in terms of plasmon resonances.

1. INTRODUCTION

Electromagnetic (EM) wave propagation in micro- and nano-structured materials has attracted considerable interest in recent years. Photonic crystals (PhCs) and metamaterials (MMs) are the two main classes of artificial optical materials [1]. In a broader sense, the PhCs may be considered as a typical example of a MM. MMs are materials synthesized from small sub-wavelength structures that are designed to strongly influence the propagation characteristic of EM fields. Usually, both feature sizes and periods of MMs are much smaller than the wavelength of light. Because the flexibility of modern nanofabrication techniques enables tailoring of the optical properties of MM, various designs for specific MM unit cells have been proposed [2–5]. The most prominent example is a combination of thin metallic wires and metallic split-ring-resonator (SRR), which have the shape of a 'U' [6–11]. The single- and multilayered metallic single-slit SRR membranes have been fabricated and their optical responses are usually studied by measuring their transmission spectra at normal incidence [12–14].

So far, many anomalous effects and applications of MM were proposed and investigated besides the negative index of refraction [15], such as inverse Snell's law [16], inverse Doppler shift [17], inverse Cerenkov effect [18, 19], perfect lens [20], optical cloaking [21, 22], and optical filter [23, 24] as well as other transformation optical devices [25, 26]. Because of its robust and predictable performance the proposed MM can be applied to tune EM resonances and provide specific local intensity enhancement. Both properties we can be used in application that utilize linear and/or nonlinear plasmon resonances [27, 28]. Application areas include surface enhanced

Raman scattering (SERS) [29, 30] and stronger second-order harmonic generation [31] which both can benefit from designable and predictable local intensity enhancement achieved by tailoring MM structure and size.

In our work, we design and investigate two MM units containing sub-wavelength double-slots — single-side double-slot (SS-DS) MM and double-side double-slot (DS-DS) MM. These two MMs are inspired by the original designs of SRRs and 'U' resonators. The main difference between our MMs and the original SRR designs is the insertion of a middle arm either on one side or on two sides of the MM unit cells. Without adding too much complexity to previously studied SRRs, this modification enables much enhanced control over the optical properties and is utilized to achieve strong local intensity enhancement at tunable resonances. Our major objective is to provide a novel MM design in order to combine simplicity in design and fabrication with flexibility and independent control over the resonant frequencies, the relative resonance strengths, and the distribution of local EM fields. Because of its flexibility and independent control over the properties of individual resonances, our MM designs can be used not only in conventional linear or nonlinear plasmon resonance applications, but can also provide resonances at several wavelengths, quasi-wavelength independent field enhancement or tunable resonances in a wide range of frequencies. All these special properties can be realized by small changes in MM size and variations of one specific design parameter such as the slot depth. The EM resonances and local intensity enhancement of these two MM types are studied by the finite-difference time-domain (FDTD) technique and the finite element method (FEM). Results show that the central-arm of the double-slot structure can not only strongly influence the frequency and distribution of the high-frequency resonance, but also enhance the local intensity of both high and low-frequency resonances. A DS-DS structure can be utilized to separately enhance the high-frequency resonance while suppressing the resonance at lower frequency. Moreover, it can dramatically increase the frequency-shift of the low-frequency resonance by changing the slots' depth. The numerical results are interpreted by the theory of plasmon resonances.

2. STRUCTURE AND SIMULATION

The cross section on y-z plane of the computational domain consisting of a single unit MM cell is shown in Fig. 1. The glass substrate is first coated with a 6 nm film of indium-tin-oxide (ITO), in order to avoid charging effects of the polymer resist layer during the exposure.

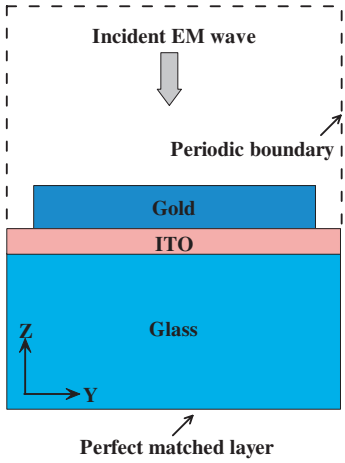

Figure 1. Cross section of the computational domain consisting of a single unit cell of the gold MM.

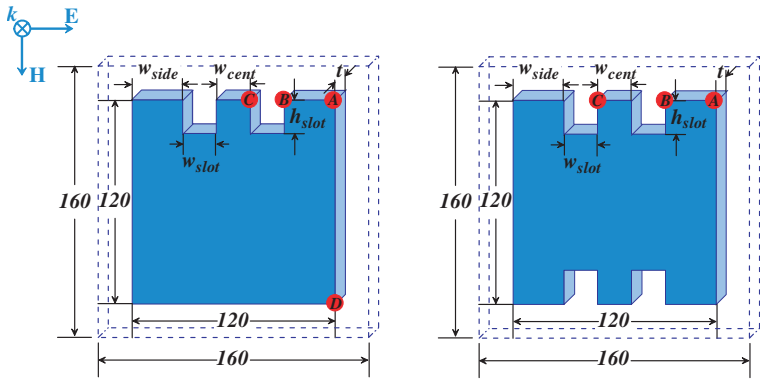

Figure 2. Landscape of (a) SS-DS MM and (b) DS-DS gold structures. The unit of the geometrical parameters is nanometer.

Afterwards, the gold structures are fabricated on top of the ITO. Fig. 2 gives the landscape of the SS-DS and DS-DS gold structures. The parameters w_{slot} and h_{slot} denote the width and depth of the sub-wavelength slots. The width of the side-arm and central-arm are w_{side} and w_{cent}, respectively. The thickness of MM gold structure is denoted by 't', which is fixed at 12 nm. To determine the local intensity enhancement, we set several monitoring points with positions indicated by red dots in Fig. 2. All of these monitoring positions are located at

the top surface of the MM structure.

The EM resonant properties and local intensity enhancement of MM are studied by three-dimensional FDTD method. The total simulation volume is $160 \times 160 \times 400\,\mathrm{nm}^3$, and the spatial mesh size is fixed at $2 \times 2 \times 2\,\mathrm{nm}^3$. The incident wave linearly polarized along the y-axis is generated by a total field/scattering field technique. Perfectly matched layers (PML) [32] are used at the top and bottom of the simulation domain to completely absorb waves leaving the simulation domain in the direction of propagation. Periodic boundary conditions are used in x and y direction. To confirm the results of the FDTD method, the electric energy density is simulated by FEM using the COMSOL Multiphysics. These two methods were cross-checked to verify their accuracy, which turn out to be consistent with each other. The thickness of the glass layer is assumed to be infinite. The permittivity of the ITO layer (glass substrate) is taken as 3.8 (2.25). For the permittivity of gold, we assume the wavelength dependence according to the Drude model [32], with the relative permittivity at infinite frequency of $\varepsilon_\infty = 9.0$, a plasma frequency of $\omega_p = 1.3166 \times 10^{16}\,\mathrm{s}^{-1}$, and a collision frequency of $\omega_c = 1.3464 \times 10^{14}\,\mathrm{s}^{-1}$ [33].

3. RESULTS AND DISCUSSION

3.1. MM with SS-DS Gold Structure

First, we investigate the MM based on a SS-DS gold structure as shown in Fig. 2(a). Fig. 3(a) gives the transmission spectra of SS-DS MMs with different central-arm widths (w_{cent}) and accordingly changed side-arm widths (w_{side}) on both sides to keep the slot width and the overall width of the structure constant.

There are three apparent resonances in the near-infrared (NIR) region. The first resonance is excited at $\bar{\nu} \approx 8,900\,\mathrm{cm}^{-1}$. In electrical engineering terms, this resonance corresponds to the so-called LC-resonance, where oscillating charges in the entire structure are excited due to the coupling between the two side-arms and the gap [6–8]. However, previous research has proven that the concept of localized surface plasmon polaritons, coupled excitations of light and electrons at a metal surface, provides a more adequate description of the physical situation considered here, where electro-magnetic fields interact with electrons confined to metal structures of sub-wavelength dimensions [34, 35]. From this point of view, the first resonance corresponds to the fundamental mode plasmon resonance. This resonance is characterized by a charge oscillation along the entire wire

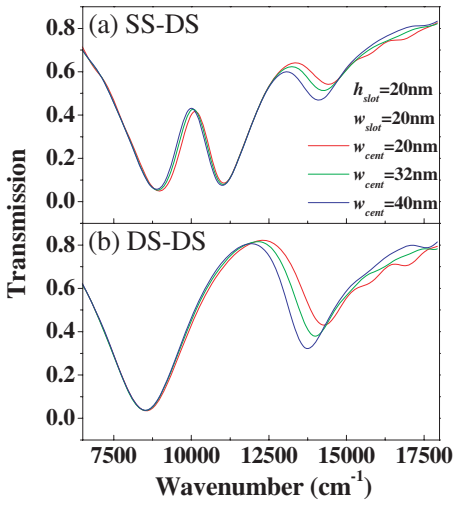

Figure 3. Transmission spectra of (a) SS-DS MM and (b) DS-DS MM for different widths of the central-arm (w_{cent}).

of the 'U' structure, which is named as U-circuit for short. In SS-DS MM, the U-circuit consists of the bottom-line and the two side-arms, but doesn't include the central-arm. The results shown in Fig. 3(a) also prove that a variation of w_{cent} has little influence on this first resonance.

The second and third resonances are observed around the frequency of $\bar{\nu} = 11,000\,\mathrm{cm}^{-1}$ and $\bar{\nu} = 14,000\,\mathrm{cm}^{-1}$, respectively. They are unambiguously related to plasmon polaritons parallel to the E-field polarization (along the y-axis). As all plasmon resonances of structures with small dimensions as considered here, their resonance frequencies depend on the ratio between the wire width and the wire thickness [35]. In SS-DS MM, the second plasmon resonance frequency depends mainly on this ratio measured along the bottom line, while the third plasmon resonance frequency is related to this width to thickness ratio along the vertical arms or along the central-arm for large w_{cent}. Therefore, the resonant frequency of the third resonance will decrease with increasing w_{cent}, while the second resonance frequency doesn't vary because of the unchanged bottom line.

To highlight the spatial distribution of local E-field and further analyze the mechanisms of these resonances, Fig. 4(a) gives the local intensity enhancement of SS-DS MM for different monitor points. First of all, the local intensity enhancement of the first resonance ($\bar{\nu} \approx 8,900\,\mathrm{cm}^{-1}$) mainly distributes on the side-arms (with monitors

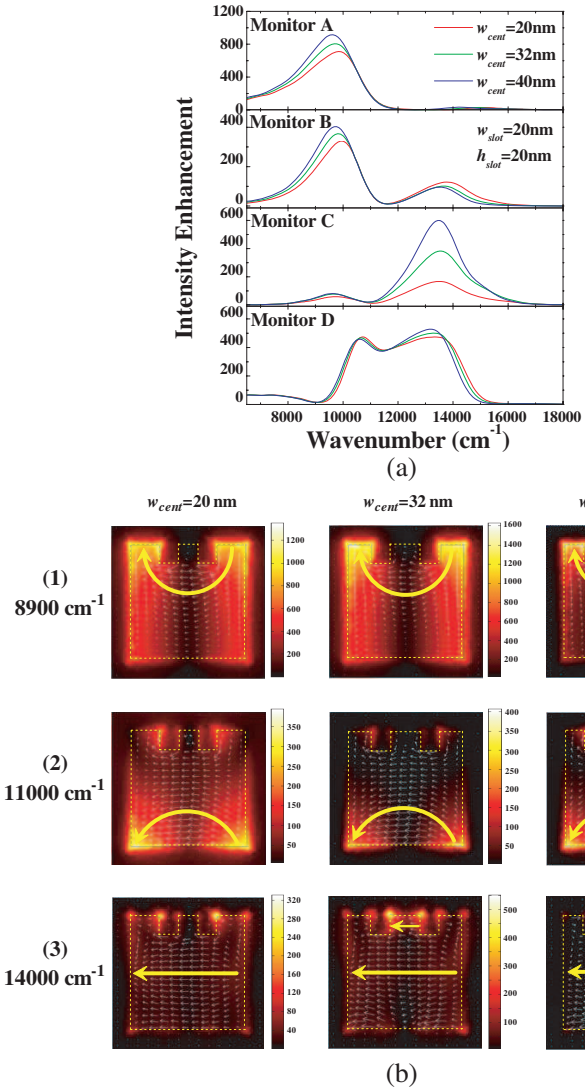

Figure 4. (a) Local intensity enhancement of the SS-DS MM for different monitor positions (see Fig. 2(a) for monitor locations). (b) The electric energy density (by colour) and the electric displacement (by arrow) of the SS-DS MM for the three plasmon resonances at w_{cent} = 20 nm, 32 nm and 40 nm, respectively. The results are normalized relative to the incident E-field. The indicative yellow arrows are added to mark the dominant direction of the electric displacement.

A and B), which are the tips of the U-circuit. With increasing of w_{cent} and decreasing of w_{side} simultaneously, this enhancement will be improved as the result of increasing of the current density in side-arms. Secondly, the local intensity enhancement of the second resonance ($\bar{\nu} \approx 11,000\,\mathrm{cm}^{-1}$) is mainly distributed around monitor D and has minors change, which is decided by the depolarization E-field in bottom line. Finally, the local intensity enhancement of the third resonance ($\bar{\nu} \approx 14,000\,\mathrm{cm}^{-1}$) increases at monitor C, while decreases at monitor B at the same time. Therefore, we can conclude that the third resonance should be excited by three vertical arms, but the resonance in the central-arm is stronger than that of side-arms. As w_{cent} increases, the local intensity enhancement of the third resonance is extracted from side-arms (monitor B) to the central-arm (monitor C) and enhanced at the same time.

To gain more inside about the under laying physics, we calculate the distribution of the electric energy density (by colour) and the electric displacement (by arrow) for different resonances by FEM (as shown in Fig. 4(b)), where the central slot width w_{cent} has been chosen as 20 nm, 32 nm and 40 nm, respectively. Indicative yellow arrows are added to highlight the dominant direction of the electric displacement. We can see that the results obtained by FDTD and FEM agree very well with each other. The electric energy density at the first resonance ($\bar{\nu} \approx 8,900\,\mathrm{cm}^{-1}$) is concentrated along the two side-arms and this concentration is enhanced with increasing w_{cent}. The distribution of electric displacement also shows that the polarization charge is mainly distributed along the side-arms. For the second resonance ($\bar{\nu} \approx 11,000\,\mathrm{cm}^{-1}$), the electric energy density is mainly concentrated at the bottom corners. Most of the electric displacement arrows point from one bottom corner to the other bottom corner, which is emphasized by the wide yellow arrows included in Fig. 4(b). The field at the third resonance ($\bar{\nu} \approx 14,000\,\mathrm{cm}^{-1}$) is very strongly localized at the corners of the slots. Interestingly, with increasing w_{cent} the intensity maxima move from the side-arm corners to the central-arm corners. This is accompanied by a further increase of the local field intensity. These very different field distributions also indicate that inserting the central-arm and changing its width can be utilized to tune the high-frequency plasmon resonance almost independently. The electric displacement direction at the third resonance is not as pronounced as at the other two resonances. Here, it's the charges are mainly distributes on the two sides of the MM and the electric displacement direction points basically from on side to the other parallel to the bottom line. Increasing w_{cent}, the electric displacement within the central-arm becomes more aligned with the overall displacement direction.

Table 1. Plasmon frequency of each resonance of SS-DS MM and DS-DS MM for various MM periodicities.

	Periodic size	Plasmon frequency		
		1st	2nd	3rd
SS-DS	150 nm	$8743\,\mathrm{cm}^{-1}$	$10780\,\mathrm{cm}^{-1}$	$14506\,\mathrm{cm}^{-1}$
	160 nm	$8924\,\mathrm{cm}^{-1}$	$11045\,\mathrm{cm}^{-1}$	$14518\,\mathrm{cm}^{-1}$
	170 nm	$9002\,\mathrm{cm}^{-1}$	$11158\,\mathrm{cm}^{-1}$	$14510\,\mathrm{cm}^{-1}$
DS-DS	150 nm	$8436\,\mathrm{cm}^{-1}$	-	$14312\,\mathrm{cm}^{-1}$
	160 nm	$8554\,\mathrm{cm}^{-1}$	-	$14314\,\mathrm{cm}^{-1}$
	170 nm	$8605\,\mathrm{cm}^{-1}$	-	$14293\,\mathrm{cm}^{-1}$

To clarify the interactions between different SS-DS units within the MM, i.e., to understand the influence of the neighborhood on the resonances of individual MM units, transmission spectra of SS-DS MMs with varying spacing periods have been calculated. The positions of every resonance for different periods are given in Table 1. From these data, we can see that the space between two adjacent units will only slightly influence the frequency of the resonances. For larger periods the frequencies of the first and second resonances increase for larger periods, which can be explained by the reduced interaction of two neighboring MM units parallel to the E-field (polarization along y-axis) [36]. For the third resonance, whose contribution part is the central-arm, the resonance frequency is basically independent of the periodicity, which might be explained by a shielding effect of the two side-arms that prevents interaction between the MM units.

3.2. MM with DS-DS Gold Structure

To increase the flexibility regarding resonance wavelengths of the MM, we designed gold units that consist of double-slots on two opposite sides, as shown in Fig. 2(b). The transmission spectra of DS-DS MM for different w_{cent} are given in Fig. 3(b), and there are obvious differences comparing with that of SS-DS MM.

Firstly, the second resonance ($\bar{\nu} \approx 11,000\,\mathrm{cm}^{-1}$) disappears in DS-DS MM because the bottom line is discontinued due to the slots and the induction current is interrupted. Secondly, because the number of vertical arms is doubled, the third resonance ($\bar{\nu} \approx 14,000\,\mathrm{cm}^{-1}$) of DS-DS MM is much stronger than that of SS-DS MM, while the frequencies of the third resonance in SS-DS and DS-DS MMs with the same w_{cent}

are almost identical. Finally, the fundamental mode resonance of DS-DS MM is around $\bar{\nu} \approx 8,500\,\mathrm{cm}^{-1}$, which is about $400\,\mathrm{cm}^{-1}$ lower than that of the SS-DS MM. In DS-DS MM, there are basically two U-circuits that are not separate, but couple with each other. As a result, the effective oscillation length of the fundamental mode resonance is increased and the resonance shifts to a lower frequency. However, the oscillation length of the U-circuits and any coupling effect will not be influenced by changes in w_{cent}, so that the fundamental mode resonance does not shift with changing w_{cent}.

To analyze the bulk properties of the proposed MM, the effective permittivity ε and refractive index n of the SS-DS and the DS-DS were calculated from the complex transmission and reflection coefficients through a single MM layer using the procedure described in Reference [37]. The peaks of the real part of the effective permittivity (Figs. 5(a) and (c)) correspond to the plasmonic resonances, i.e., the transmission minima in Fig. 3. As shown in Figs. 5(b) and (d), negative refractive indices appear at wavenumbers just below

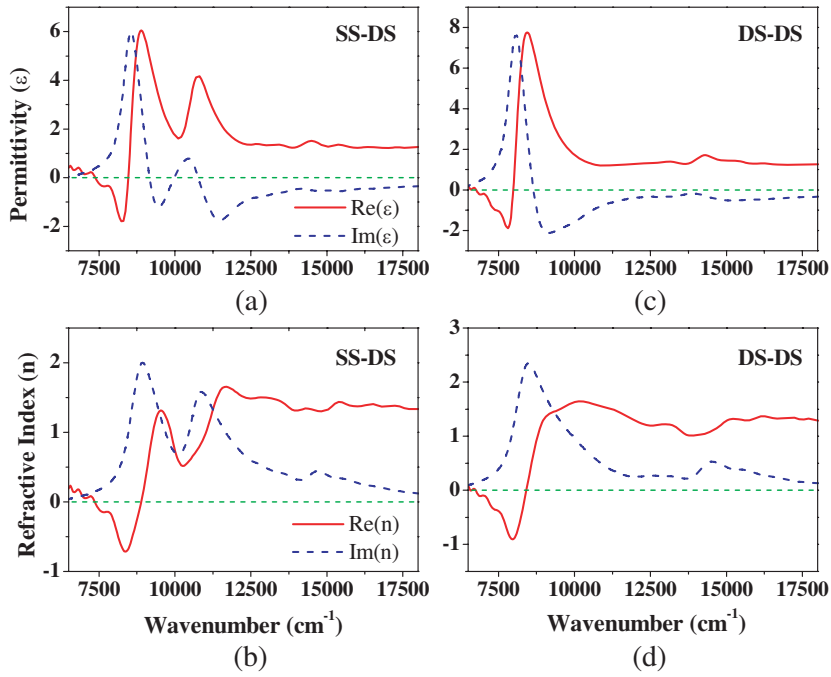

Figure 5. Extracted effective permittivity ε ((a) and (c)) and refractive index n ((b) and (d)) of the SS-DS and DS-DS. $h_{slot} = 20\,\mathrm{nm}$, $w_{slot} = 20\,\mathrm{nm}$, and $w_{cent} = 20\,\mathrm{nm}$, respectively.

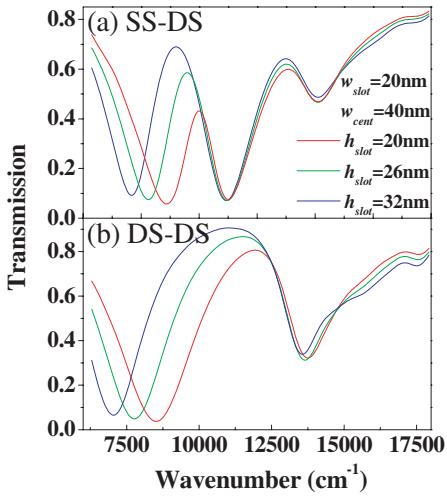

Figure 6. Transmission spectra of (a) SS-DS and (b) DS-DS MMs for different slot depths (h_{slot}).

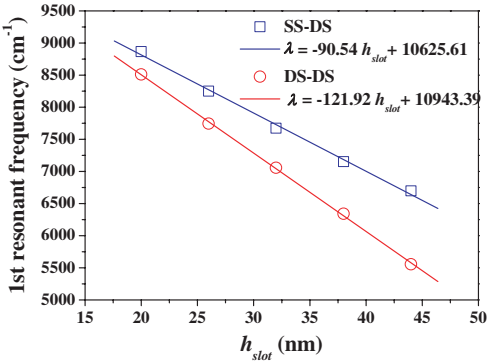

Figure 7. Wavenumber of the first resonance for DS-DS MM and SS-DS MM as the function of h_{slot}.

the first resonances, which are caused by the respective LC electrical resonances.

To investigate the influence of the double-side slot structure, Fig. 6 shows the transmission spectra of the SS-DS and DS-DS MMs for the different depths of the slot (h_{slot}). Results show that only the first resonance both in SS-DS and DS-DS MMs is strongly affected and has a clear shift. Fig. 7 gives the frequency shift of the first resonance for DS-DS and SS-DS MMs as the function of h_{slot}. We can conclude that

the frequency shift of the first resonance for SS-DS and DS-DS MMs can be approximated by a linear dependence. The slope of DS-DS is steeper than that of SS-DS MM, i.e., the red-shift of DS-DS MM is faster than that of SS-DS MM. As the oscillation length of the U-circuit is increased with increasing h_{slot}, the first resonance will shift to lower frequencies. For DS-DS MM, the oscillation length of each single U-circuit and the coupling effect between the two circuits can be increased and enhanced by increasing h_{slot}, respectively. Therefore, the red-shift of the first resonance in DS-DS MM is faster than that in SS-DS MM. This result also confirms our statement about the coupling effect between two circuits in DS-DS MM. In addition, h_{slot} does not affect the other resonances because the oscillation distance of the free electrons in the E-field polarization direction is not influenced. That is, the fundamental mode resonance can be independently tuned by changing h_{slot}.

Figure 8(a) shows the local intensity enhancement of the DS-DS MM at different monitor positions. Similar to Fig. 4(b) for the SS-DS MM, Fig. 8(b) gives the distribution of the electric energy density (by colour) and the electric displacement (by arrow) in the DS-DS MM at the two plasmon resonances obtained by FEM. The local intensity enhancements at $\bar{\nu} \approx 8,500\,\mathrm{cm}^{-1}$ and $\bar{\nu} \approx 14,000\,\mathrm{cm}^{-1}$ are detected at the monitor positions A, B and B, C, respectively. With increasing central arm width w_{cent} in the DS-DS MM, the local intensity maxima at the resonance around $\bar{\nu} = 14,000\,\mathrm{cm}^{-1}$ also move from side-arm corners to the central-arm corners as observed for the SS-DS MM. Meanwhile, the achievable local intensity enhancements at both resonances ($\bar{\nu} \approx 8,500\,\mathrm{cm}^{-1}$, $\bar{\nu} \approx 14,000\,\mathrm{cm}^{-1}$ are increasing for larger w_{cent}. However, the local intensity enhancement at $\bar{\nu} \approx 8,500\,\mathrm{cm}^{-1}$ is a little bit lower than that of SS-DS MM because of the doubled number of U-circuits and the decreasing of the current density in each U-circuit. The distributions of the electric energy in the DS-DS MM are somewhat similar to those of SS-DS MM with strong concentrations in the corners and along the side arms at the first resonance ($\bar{\nu} \approx 8,500\,\mathrm{cm}^{-1}$). The electric displacement calculated at the second resonance ($\bar{\nu} = 14,000\,\mathrm{cm}^{-1}$) very much resembles the behavior at the third resonance of the SS-DM shown in Fig. 4(b).

Changes of the resonance frequencies caused by the interaction between neighboring DS-DS MM units are also given in Table 1. As in the SS-DS MM case, the frequency of the first resonance is increased at larger periods, i.e., larger spacing between individual MM units, while the plasmon frequency of the third resonance changes little. The reason for these phenomena is the same as in the SS-DS MM case.

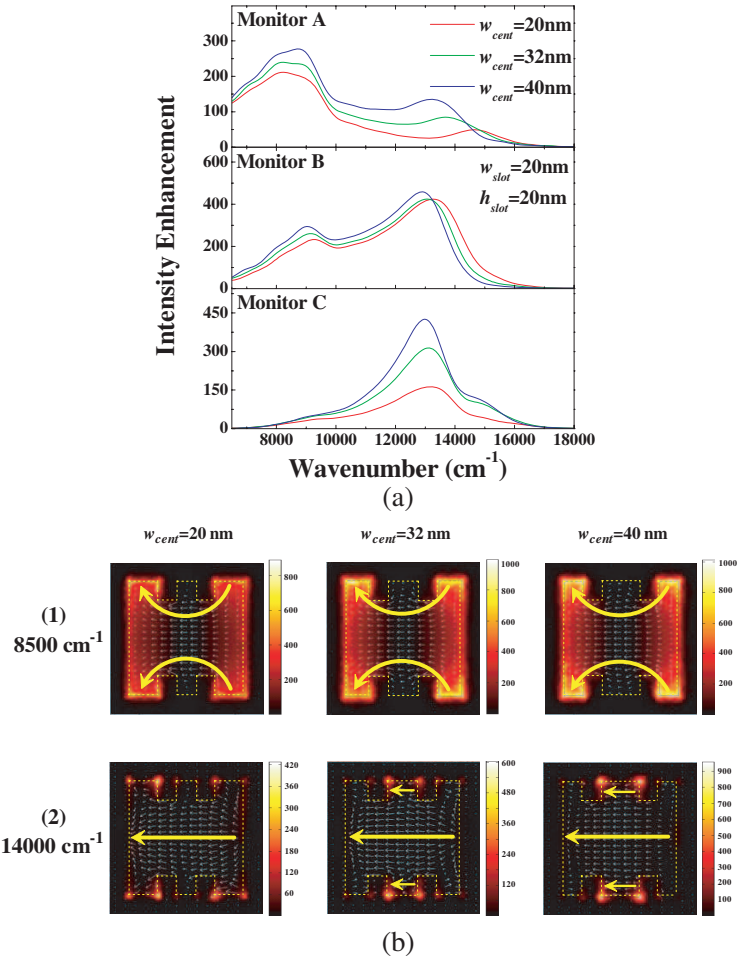

Figure 8. (a) Local intensity enhancement of the DS-DS MM for different monitor positions (see Fig. 2(b) for monitor locations). (b) The electric energy density of the DS-DS MM for the two plasmon resonances when w_{cent} = 20 nm, 32 nm and 40 nm, respectively. The results are normalized relative to the incident E-field.

4. CONCLUSIONS

In this paper, we propose two unit cells for MM that contains sub-wavelength double-slots and exhibit strong EM resonances in the NIR region. Using the FDTD and FEM methods, we demonstrate predictably the tunability of the EM resonances through structural

changes and analyze local intensity enhancement at resonance frequencies. Our results show that both structures are well-suited to tailor the EM resonances. In particular, the central-arm of the double-slot can influence the frequency and strength of the high-frequency resonances and enhance local intensities at both high and low-frequency resonances. A DS-DS structure can be utilized to separately enhance the high-frequency resonance at shorter wavelength while suppressing the resonance at lower frequency. At the same time, a change in the slot depth can be used to widely tune the fundamental mode resonance without much affecting on the higher order mode resonances. Moreover, periodic parameter also influences the resonant frequency for both SS-DS and DS-DS MM structures.

ACKNOWLEDGMENT

This research is supported by the National Sciences Foundation (No. 0725479), the state of Arizona TRIF Photonics Initiative, China 973 program (No. 2006CB302904), Chinese National Key Basic Research Special Fund (No. 2011CB922003), Natural Science Foundation of China (No. 90923035 and No. 61008002), the Specialized Research Fund for the Doctoral Program of Higher Education (No. 20100031120005), and the Fundamental Research Funds for the Central Universities.

REFERENCES

1. Joannopoulos, J. D., *Photonic Crystals: Molding the Flow of Light*, Princeton University Press, 1995.
2. Shalaev, V. M., W. Cai, U. K. Chettiar, H. K. Yuan, A. K. Sarychev, V. P. Drachev, and A. V. Kildishev, "Negative index of refraction in optical metamaterials," *Opt. Lett.*, Vol. 30, 3356–3358, 2005.
3. Dolling, G., C. Enkrich, M. Wegener, J. F. Zhou, C. M. Soukoulis, and S. Linden, "Cut-wire pairs and plate pairs as magnetic atoms for optical metamaterials," *Opt. Lett.*, Vol. 30, 3198–3200, 2005.
4. Zhang, S., W. Fan, N. C. Panoiu, K. J. Malloy, R. M. Osgood, and S. R. J. Brueck, "Experimental demonstration of near-infrared negative-index metamaterials," *Phys. Rev. Lett.*, Vol. 95, 137404, 2005.
5. Sabah, C., "Tunable metamaterial design composed of triangular split ring resonator and wire strip for S- and C- microwave bands," *Progress In Electromagnetics Research B*, Vol. 22, 341–357, 2010.

6. Katsarakis, N., T. Koschny, M. Kafesaki, E. N. Economou, and C. M. Soukoulis, "Electric coupling to the magnetic resonance of split ring resonators," *Appl. Phys. Lett.*, Vol. 84, 2943–2945, 2004.
7. Katsarakis, N., G. Konstantinidis, A. Kostopoulos, R. S. Penciu, T. F. Gundogdu, M. Kafesaki, E. N. Economou, T. Koschny, and C. M. Soukoulis, "Magnetic response of split-ring resonators in the far-infrared frequency regime," *Opt. Lett.*, Vol. 30, 1348–1350, 2005.
8. Linden, S., C. Enkrich, M. Wegener, J. F. Zhou, T. Koschny, and C. M. Soukoulis, "Magnetic response of metamaterials at 100 Terahertz," *Science*, Vol. 306, 1351–1353, 2004.
9. Marqués, R., F. Martín, and M. Sorolla, *Metamaterials with Negative Parameters*, Wiley, New York, 2008.
10. Solymar, L. and E. Shamonina, *Waves in Metamaterials*, Oxford University, New York, 2009.
11. Zeng, Y., C. Dineen, and J. V. Moloney, "Magnetic dipole moments in single and coupled split-ring resonators," *Phys. Rev. B*, Vol. 81, 075116, 2010.
12. Gansel, J. K., M. Thiel, M. S. Rill, M. Decker, K. Bade, V. Saile, G. von Freymann, S. Linden, and M. Wegener, "Gold helix photonic metamaterial as broadband circular polarizer," *Science*, Vol. 325, 1513–1515, 2009.
13. Liu, N., H. Liu, S. Zhu, and H. Giessen, "Stereometamaterials," *Nat. Photonics*, Vol. 3, 157–162, 2009.
14. Sersic, I., M. Frimmer, E. Verhagen, and A. F. Koenderink, "Electric and magnetic dipole coupling in near-infrared split-ring metamaterial arrays," *Phys. Rev. Lett.*, Vol. 103, 213902, 2009.
15. Smith, D. R., J. B. Pendry, and M. C. K. Wiltshire, "Metamaterials and negative refractive index," *Science*, Vol. 305, 788–792, 2004.
16. Houck, A. A., J. B. Brock, and I. L. Chuang, "Experimental observations of a left-handed material that obeys Snell's law," *Phys. Rev. Lett.*, Vol. 90, 137401, 2003.
17. Seddon, N. and T. Bearpark, "Observation of the inverse Doppler effect," *Science*, Vol. 302, 1537–1540, 2003.
18. Lu, J., T. M. Grzegorczyk, Y. Zhang, J. Pacheco, B. I. Wu, J. A. Kong, and M. Chen, "Cerenkov radiation in materials with negative permittivity and permeability," *Opt. Express*, Vol. 11, 723–734, 2003.
19. Duan, Z.-Y., B.-I. Wu, S. Xi, H. Chen, and M. Chen, "Research progress in reversed cherenkov radiation in double-negative

metamaterials," *Progress In Electromagnetics Research*, Vol. 90, 75–87, 2009.

20. Pendry, J. B., "Negative refraction makes a perfect lens," *Phys. Rev. Lett.*, Vol. 85, 3966–3969, 2000.
21. Schurig, D., J. J. Mock, B. J. Justice, S. A. Cummer, J. B. Pendry, A. F. Starr, and D. R. Smith, "Metamaterial electromagnetic cloak at microwave frequencies," *Science*, Vol. 314, 977–980, 2006.
22. Leonhardt, U., "Optical conformal mapping," *Science*, Vol. 312, 1777–1780, 2006.
23. Navarro-Cia, M., J. M. Carrasco, M. Beruete, and F. J. Falcone, "Ultra-wideband metamaterial filter based on electroinductive-wave coupling between microstrips," *Progress In Electromagnetics Research Letters*, Vol. 12, 141–150, 2009.
24. NaghshvarianJahromi, M., "Novel compact meta-material tunable quasi elliptic band-pass filter using microstrip to slotline transition," *Journal of Electromagnetic Waves and Applications*, Vol 24, No. 17–18, 2371–2382, 2010.
25. Rahm, M., D. Schurig, D. A. Roberts, S. A. Cummer, D. R. Smith, and J. B. Pendry, "Design of electromagnetic cloaks and concentrators using form-invariant coordinate transformations of Maxwell's equations," *Photonics Nanostruct. Fundam. Appl.*, Vol. 6, 87–95, 2008.
26. Kwon, D.-H. and D. H. Werner, "Transformation optical designs for wave collimators, flat lenses and right-angle bends," *New J. Phys.*, Vol. 10, 115023, 2008.
27. Zharov, A., I. V. Shadrivov, and Y. S. Kivshar, "Nonlinear properties of left-handed metamaterials," *Phys. Rev. Lett.*, Vol. 91, 037401, 2003.
28. Liu, Y., G. Bartal, D. A. Genov, and X. Zhang, "Subwavelength discrete solitons in nonlinear metamaterials," *Phys. Rev. Lett.*, Vol. 99, 153901, 2007.
29. Chen, S., L. Han, A. Schülzgen, H. Li, L. Li, J. V. Moloney, and N. Peyghambarian, "Local electric field enhancement and polarization effects in a surface-enhanced raman scattering fiber sensor with chessboard nanostructure," *Opt. Express*, Vol. 16, 13016–13023, 2008.
30. Zeng, Y., Q. Wu, and D. H. Werner, "Electrostatic theory for designing lossless negative permittivity metamaterials," *Opt. Lett.*, Vol. 35, 1431–1433, 2010.
31. Klein, M. W., C. Enkrich, M. Wegener, and S. Linden, "Second-harmonic generation from magnetic metamaterials," *Science*,

Vol. 313, 502–504, 2006.

32. Taflove, A. and S. C. Hagness, *Computational Electrodynamics — The Finite-difference Time-domain Method*, Artech House, Boston, 2005.
33. Palik, E. D., *Handbook of Optical Constants of Solids*, Academic, New York, 1985.
34. Ditlbacher, H., A. Hohenau, D. Wagner, U. Kreibig, M. Rogers, F. Hofer, F. R. Aussenegg, and J. R. Krenn, "Silver nanowires as surface plasmon resonators," *Phys. Rev. Lett.*, Vol. 95, 257403, 2005.
35. Rockstuhl, C., F. Lederer, C. Etrich, T. Zentgraf, J. Kuhl, and H. Giessen, "On the reinterpretation of resonances in split-ring-resonators at normal incidence," *Opt. Express*, Vol. 14, 8827–8836, 2006.
36. Rockstuhl, C., T. Zentgraf, H. Guo, N. Liu, C. Etrich, I. Loa, K. Syassen, J. Kuhl, F. Lederer, and H. Giessen, "Resonances of split-ring resonator metamaterials in the near infrared," *Appl. Phys. B*, Vol. 84, 219–227, 2006.
37. Szabó, Z., G.-H. Park, R. Hedge, and E.-P. Li, "A unique extraction of metamaterial parameters based on kramers-kronig relationship," *IEEE T. Microw. Theory*, Vol. 58, 2646–2653, 2010.